

MoEDAL search in the CMS beam pipe for magnetic monopoles produced via the Schwinger effect

B. Acharya,^{1, a} J. Alexandre,¹ P. Benes,² B. Bergmann,² S. Bertolucci,³ A. Bevan,⁴ R. Brancaccio,⁵ H. Branzas,⁶ P. Burian,² M. Campbell,⁷ S. Cecchini,³ Y. M. Cho,⁸ M. de Montigny,⁹ A. De Roeck,⁷ J. R. Ellis,^{1, 10} M. Fairbairn,¹ D. Felea,⁶ M. Frank,¹¹ O. Gould,¹² J. Hays,⁴ A.M. Hirt,¹³ D. L.-J. Ho,¹⁴ P. Q. Hung,¹⁵ J. Janecek,² M. Kalliokoski,¹⁶ D. H. Lacarrère,⁷ C. Leroy,¹⁷ G. Levi,⁵ A. Margiotta,⁵ R. Maselek,¹⁸ A. Maulik,^{3, 9} N. Mauri,⁵ N. E. Mavromatos,^{1, b} L. Millward,⁴ V. A. Mitsou,^{19, b} E. Musumeci,¹⁹ I. Ostrovskiy,^{20, c} P.-P. Ouimet,²¹ J. Papavassiliou,¹⁹ L. Patrizii,³ G. E. Pāvālaš,⁶ J. L. Pinfold,⁹ L. A. Popa,⁶ V. Popa,⁶ M. Pozzato,³ S. Pospisil,² A. Rajantie,¹⁴ R. Ruiz de Austri,¹⁹ Z. Sahnoun,⁵ M. Sakellariadou,¹ K. Sakurai,¹⁸ S. Sarkar,¹ G. Semenoff,²² A. Shaa,⁹ G. Sirri,³ K. Sliwa,²³ R. Soluk,⁹ M. Spurio,⁵ M. Staelens,¹⁹ M. Suk,² M. Tenti,³ V. Togo,³ J. A. Tuszyński,⁹ A. Upreti,²⁰ V. Vento,¹⁹ and O. Vives¹⁹

¹*Theoretical Particle Physics & Cosmology Group, Physics Dept., King's College London, UK*

²*IEAP, Czech Technical University in Prague, Czech Republic*

³*INFN, Section of Bologna, Bologna, Italy*

⁴*School of Physics and Astronomy, Queen Mary University of London, UK*

⁵*INFN, Section of Bologna & Department of Physics & Astronomy, University of Bologna, Italy*

⁶*Institute of Space Science, Bucharest - Magurele, Romania*

⁷*Experimental Physics Department, CERN, Geneva, Switzerland*

⁸*Center for Quantum Spacetime, Sogang University, Seoul, Korea*

⁹*Physics Department, University of Alberta, Edmonton, Alberta, Canada*

¹⁰*Theoretical Physics Department, CERN, Geneva, Switzerland*

¹¹*Department of Physics, Concordia University, Montreal, Quebec, Canada*

¹²*University of Nottingham, Nottingham, UK*

¹³*Department of Earth Sciences, Swiss Federal Institute of Technology, Zurich, Switzerland*

¹⁴*Department of Physics, Imperial College London, UK*

¹⁵*Department of Physics, University of Virginia, Charlottesville, VA, USA*

¹⁶*Helsinki Institute of Physics, University of Helsinki, Helsinki, Finland*

¹⁷*Departement de Physique, Université de Montreal, Quebec, Canada*

¹⁸*Institute of Theoretical Physics, University of Warsaw, Warsaw, Poland*

¹⁹*IFIC, Universitat de Valencia - CSIC, Valencia, Spain*

²⁰*Department of Physics and Astronomy, University of Alabama, Tuscaloosa, Alabama, USA*

²¹*Physics Department, University of Regina, Regina, Saskatchewan, Canada*

²²*Department of Physics, University of British Columbia, Vancouver, British Columbia, Canada*

²³*Department of Physics and Astronomy, Tufts University, Medford, Massachusetts, USA*

(Dated: February 27, 2024)

We report on a search for magnetic monopoles (MMs) produced in ultraperipheral Pb–Pb collisions during Run-1 of the LHC. The beam pipe surrounding the interaction region of the CMS experiment was exposed to $174.29 \mu\text{b}^{-1}$ of Pb–Pb collisions at 2.76 TeV center-of-mass energy per collision in December 2011. It was scanned by the MoEDAL experiment using a SQUID magnetometer to search for trapped MMs. No MM signal was observed. The two distinctive features of this search are the use of a trapping volume very close to the collision point and ultra-high magnetic fields generated during the heavy-ion run that could produce MMs via the Schwinger effect. These two advantages allowed setting the first reliable, world-leading mass limits on MMs with high magnetic charge. In particular, the established limits are the strongest available in the range between 2 and 45 Dirac units, excluding MMs with masses of up to 80 GeV at 95% confidence level.

The symmetry of the Maxwell's equations under exchange of the electric and magnetic fields, currently apparent only in vacuum, would be restored if isolated magnetic charges, or magnetic monopoles (MMs), exist. The presence of MMs could explain the quantization of the electric charge, as shown by Dirac [1]. Dirac's argument also requires the magnetic charge to be quantized, with the fundamental unit of $g_D = 2\pi\hbar/e$, the Dirac charge. Further motivation for MMs is provided by a number of Grand Unified Theories (GUTs) [2, 3] and other beyond the standard model (BSM) scenarios [4–11] that contain

topologically stable, finite-energy MM solutions, some with expected masses on the order of TeV. Importantly, in such models the fundamental magnetic charge is predicted to be twice or thrice larger than the Dirac charge, the latter possibility realized if the MM does not carry magnetic color charge [12]. In general, the value of the minimum magnetic charge depends on the global properties of the gauge group of the underlying theory [13], with an $SU(N)$ theory typically giving rise to a minimal magnetic charge of N Dirac units. Finding the minimum magnetic charge could provide a unique way to probe the

structure of the gauge group. Finally, MMs predicted in string theories are also required to have a fundamental magnetic charge equal to an integer multiple of the Dirac value, as shown by Wen and Witten [14].

The motivation for the existence of MMs has led to an array of direct searches utilizing a wide range of techniques and tuned to very different MM velocity and mass ranges (for a recent review, see [15]). However, many of the searches were limited to smaller magnetic charges, as the ionization losses of MMs in matter increase rapidly with magnetic charge, leading to loss of detection efficiency due to MM absorption in passive materials or electronics saturation effects. One way to increase sensitivity to high magnetic charges is to use an accelerator beam pipe as an MM trapping volume [16, 17], an approach that allowed the H1, D0, and CDF collaborations to establish limits on MMs with up to six units of Dirac charge [18–20]. Another exception to the limitation is the MoEDAL experiment, whose dedicated sensitivity to high ionization allowed it to set limits on particles with magnetic charge of up to five g_D [21, 22]. The most recent MoEDAL result has extended the sensitivity to ten units of Dirac charge [23].

An additional difficulty of most collider experiments to date is establishing reliable mass limits on MM production. Due to the large coupling of MMs to photons, perturbation theory could not be used to calculate the production cross section of MMs in elementary particle collisions unless appropriate resummation schemes are applied [24]. It is also expected that the production of composite monopoles — the type predicted by the GUT and BSM models — is exponentially suppressed by a factor of $e^{-\mathcal{O}(500)}$ in such collisions [25, 26] due to a negligible overlap between the initial and final states. These two limitations were recently overcome by a search for MM production in ultraperipheral collisions of lead ions at the LHC via the Schwinger effect [27]. The Schwinger production cross section is calculable nonperturbatively, and the production of composite MMs is actually enhanced compared to elementary MMs [28, 29]. This search established limits for MMs with up to three units of Dirac charge, with sensitivity to higher charges hampered by the absorption of the highly-ionizing MMs by passive materials before they could reach the detectors.

In order to extend greatly the sensitivity to high magnetic charge while still being able to calculate reliably the production cross section, we search for MMs trapped in the CMS beam pipe during heavy-ion collisions. The beam pipe was exposed to Pb–Pb collisions at $\sqrt{S_{NN}} = 2.76$ TeV with an integrated luminosity of $174.29 \mu\text{b}^{-1}$ during Run-1 of the LHC. The beryllium pipe is 1 mm thick and extends 1902 mm in both directions from the interaction point. The CMS solenoid provided a near-uniform 3.7–3.8 T magnetic field at the location of the pipe [30].

The peak strength of the fleeting magnetic field gen-

erated during the ultraperipheral collisions is calculated following the approach described in Ref. [29]. The field is characterised by its peak strength, B , and inverse decay time, ω , estimated as

$$B \approx c_B \frac{Zev\gamma}{2\pi R_{\text{Pb}}^2}, \quad \omega \approx c_\omega \frac{v\gamma}{R}, \quad (1)$$

where $R_{\text{Pb}} = (6.62 \pm 0.06)$ fm is the lead ion radius, Z is the lead ion charge, $v \approx 1$ is the ion velocity, γ is the corresponding Lorentz factor, c_B and c_ω are $O(1)$ numerical coefficients. For Run-1 Pb–Pb collisions, $B = (2.1 \pm 0.1) \cdot 10^{16}$ T and $\omega = (6.1 \pm 0.3) \cdot 10^{25}$ s $^{-1}$.

The production cross section and center-of-mass kinematics are calculated following the formalism developed in Refs. [28, 29]. These references describe two approximate approaches — the free particle approximation (FPA) and the locally constant field approximation (LCFA). The FPA approximation considers the spacetime dependence of the electromagnetic fields generated during a collision to all orders but ignores the MM pair’s self-interactions. Conversely, the LCFA approximation considers self-interactions to all orders but neglects the spacetime dependence of the electromagnetic field. Both approaches provide conservative lower limits on the production cross section, as including the self-interactions and fields’ spacetime dependence has been shown to increase the MM production [28, 29]. For high magnetic charges, the LCFA is expected to be more reliable, as self-interactions become more important, and because the instanton for MM production shrinks, so that spacetime dependence becomes less important at higher charges [29]. Consequently, this work uses the LCFA cross section shown in Eq. (2) as a function of the MM mass, M , and magnetic charge, g .

$$\sigma_{\text{LCFA}} = \theta(F - 2M) \frac{2(gB)^{9/2} R_{\text{Pb}}^4}{9\pi^2 M^5 \omega^2} \exp\left(-\frac{\pi M^2}{gB} + \frac{g^2}{4}\right). \quad (2)$$

Here θ denotes the step function and F is the total energy in the electromagnetic field available for MM pair production. The total available energy shown in Eq. (3) provides an upper limit on the mass of an MM that could be produced in a collision, regardless of the value of the cross section:

$$F = \int d^3x \frac{1}{2} (B^2 - E^2) \theta(B^2 - E^2) \Big|_{t=0}, \quad (3)$$

where B and E are the magnetic and electric fields generated during the collision, and the integral is evaluated over the collision region at the time of the closest approach. A more complete calculation of the cross section in Eq. (2) would include the backreaction effects of MM pair production on the electromagnetic fields. However, since it includes the negative contribution of the energy of the electric field, F provides a conservative estimate of the mass threshold.

The kinematics of MM production in the Pb–Pb collisions is dominated by the time dependence of the electromagnetic fields. While the LCFA is expected to describe better the total cross section, it neglects the time dependence of the field and leads to an underestimate of the width of the momentum distribution that is incompatible with the time–energy uncertainty principle. Hence, following Ref. [28], we use the FPA formalism to compute the relative momentum distribution shown in Fig. 1. The width of this distribution saturates the time–energy uncertainty principle.

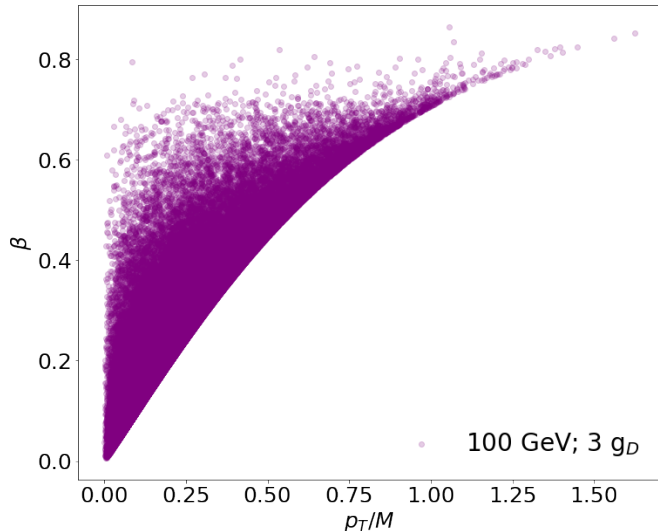


FIG. 1. An example momentum distribution for Schwinger production of MMs with three units of Dirac charge and 100 GeV mass calculated in the FPA approximation.

A detailed GEANT4 [31] Monte Carlo (MC) simulation is used to estimate the fraction of produced MMs that are captured by the beam pipe. The MMs are generated at the CMS interaction point with the momentum distribution shown in Fig. 1 and propagated through the beam pipe geometry, taking into account the effect of the CMS solenoidal magnetic field and energy losses. The MM’s electron ionization energy loss is implemented according to the formalism described in Refs. [32–34]. This provides an accurate description of total energy loss from the relativistic regime down to $\beta \sim 10^{-3}$. The nuclear stopping power, which increases the total loss by $\sim 1\%$ at $\beta=10^{-2}$, has been included in this work following Ref. [34]. For diamagnetic materials like beryllium, another contribution to the energy loss becomes relevant below $\beta \sim 10^{-3}$ [35] and was implemented here for MMs with magnetic charges $\leq 2 g_D$. The nuclear and diamagnetic components of the total energy loss were found to have insignificant effects on the results.

Once inside the beam pipe, the MMs begin to lose energy. However, the energy losses in beryllium are insufficient to counteract the acceleration by the CMS mag-

netic field. Therefore, the only MMs (or anti-MMs) that could potentially get trapped in the beam pipe were those produced with an initial momentum directed against (or along) the field lines. Such MMs are decelerated by the field and eventually turn around toward the field’s direction. If, at the instant of turning, the MM’s position is within the beam pipe volume, then it would reach its lowest kinetic energy inside the beam pipe material. If this kinetic energy is less than the expected binding energy, the MM is expected to be trapped. According to Ref. [36], an MM would disrupt the beryllium nucleus and bind to its constituents. Among the different thresholds on binding energy — binding to an individual proton or neutron, or all nine nucleons comprising the nucleus — the conservative scenario is binding to a single proton, with a calculated binding energy of 15.1 keV [37], increasing to 1 MeV if the proton’s form factor is taken into account [38]. Even for the conservative case of 15.1 keV binding energy, the lifetime [36] of an MM–proton bound state in the presence of the CMS external field is estimated to be very large for all values of the magnetic charge considered in this work. Fig. 2 shows the distribution of the MMs’ kinetic energies at the instant of turning within the beam pipe. The peaks in the distribution coincide with the initial angle θ relative to the beam direction that are favored by the MMs turning within the beam pipe region. Only specific initial directions of MMs with specific initial kinetic energies will result in them turning inside the beam pipe, giving rise to the features of the distribution shown in the figure.

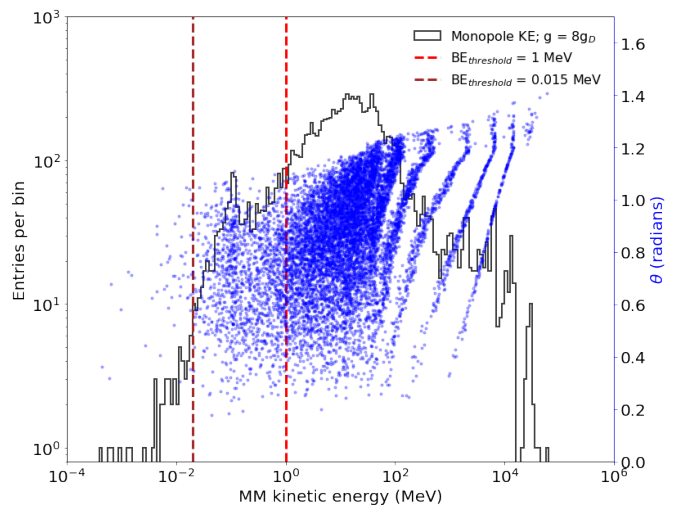


FIG. 2. The distribution of the MMs’ kinetic energies within the beam pipe at the point of turning (black line). The red line shows the assumed binding energy. The distribution of initial polar angles for MMs that turn inside the beam pipe is also shown (blue dots).

The beam pipe trapping efficiency is calculated as the ratio of the number of MMs bound to the beryllium volume to the total number of generated MMs. The trap-

ping efficiency decreases rapidly for MMs with magnetic charges below $3 g_D$, because the MMs do not lose enough energy in the 1-mm thick beam pipe and punch through. On the other hand, the efficiency also drops quickly for very high magnetic charges because they would decelerate and turn before reaching the beam pipe, since their acceleration is proportional to the magnetic charge. Thus, the trapping efficiency shown in Fig. 3 peaks at magnetic charges of 5–10 g_D .

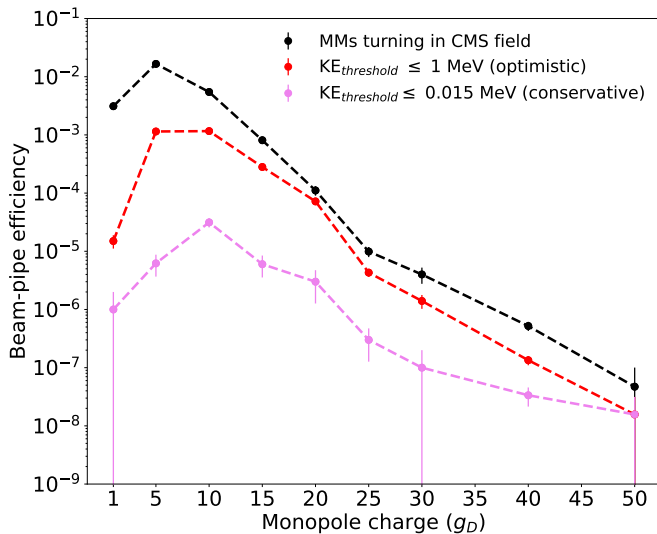


FIG. 3. The MM trapping efficiency in the CMS beam pipe as a function of the magnetic charge.

We define R_{exp} as the mean rate of MMs expected to be trapped in the beam pipe during the LHC Run-1 Pb–Pb collisions. For a particular MM mass and charge, the expected rate is calculated as a product of the trapping efficiency, the CMS integrated luminosity, and the LCFA cross-section. Two bounds on the MM–nucleus binding energy — 15.1 keV and 1.0 MeV — are used in the calculation as described earlier. Overall, the results are not very sensitive to this choice because the expected rate for charges above $2 g_D$ remains high enough that MMs with the mass corresponding to the upper limit in Eq. 3 could still be excluded in spite of the lower trapping efficiency.

The main systematic error in R_{exp} is due to the uncertainties in the magnetic field strength B and the inverse decay time ω . For Pb–Pb collisions at $\sqrt{S_{NN}}=2.76$ TeV, the peak value of $B = 4.0 \pm 0.2$ GeV² and $\omega = 40 \pm 1.7$ GeV is calculated using Eq. 1. These uncertainties, described in detail in [27], arise from the assumptions of the fit model and are reflected in the uncertainty of the results. We assume uniform distributions within these ranges of uncertainty. The final positions of MMs with identical initial momenta were checked to be stable to within 1% of the beam pipe thickness when the GEANT4’s step length and field integration parameters (ϵ_{max} , “delta intersection”, “delta one step”, and “delta-

chord”) were varied within recommended bounds [39]. The systematic uncertainty in the MM energy loss calculated using GEANT4 are 1–7% [40].

Results and conclusion. The CMS beam pipe exposed to the Pb–Pb collisions during Run-1 of the LHC was scanned for the presence of trapped MMs using a direct current SQUID long-core magnetometer installed at ETH Zurich. The presence of an MM in the sample would lead to a non-zero persistent current. Conversely, the north and south poles of a magnetic dipole passing through the magnetometer would induce currents that cancel each other out. The beryllium section of the beam pipe was cut into 171 rings of 2-cm width each. The rings were further sub-divided into fragments. The fragments from three rings were then inserted into a plastic tube of dimension 2.54 cm \times 2.54 cm \times 19 cm and scanned together. The process was then repeated for fragments from another set of three rings. A total of 57 tubes with each set of fragments were passed through the SQUID multiple times (6–12 times) to scan for the presence of magnetic charges. Fig. 4 shows the results. No statistically significant signal was observed. To calibrate the device’s response to magnetic charge, two independent methods were used, as described elsewhere [21, 40]. The existence of an MM with $|g| \geq 0.5 g_D$ in the trapping volume was excluded at more than 3σ .

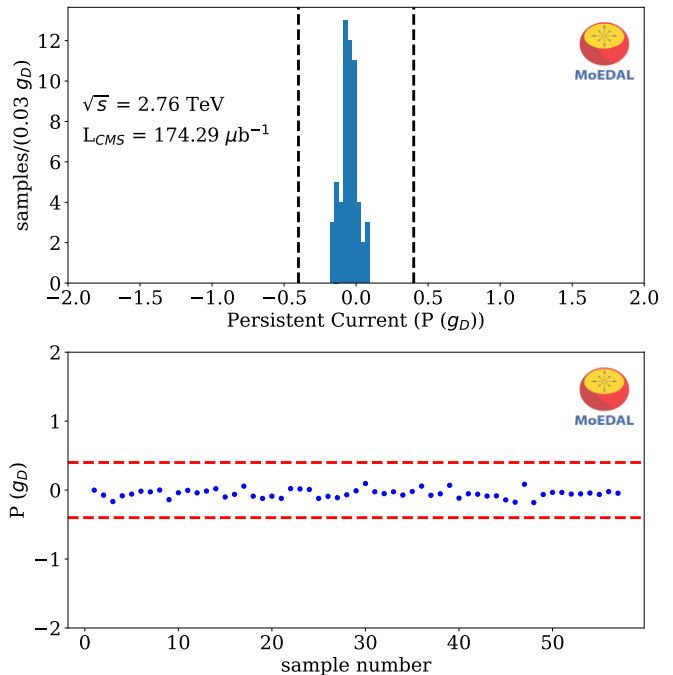


FIG. 4. (Top) Distribution of average persistent currents for the beam pipe samples. (Bottom) Average persistent current vs. sample number.

Figure 5 shows the exclusion region in the magnetic charge versus mass plane. The statistical significance of the limits is calculated from the Poisson statistics on R_{exp}

and the uncertainties involved using an approach similar to that followed in Ref. [27]. The trapping efficiency increases with increasing magnetic charge up to $6g_D$ and then starts decreasing. This is because high magnetic charges would be strongly accelerated by the CMS magnet, thus reducing the efficiency. However, the Schwinger LCFA cross-section increases with increasing magnetic charge. The mass limits remain nearly constant because the mass of MMs that could be produced in Pb–Pb Run-1 collisions is limited by the energy in the electromagnetic field, calculated using Eq. (3).

Our analysis combines the advantages of searching for MM production in heavy-ion collisions via the Schwinger effect with using a beam pipe as a trapping volume, which leads to unprecedented sensitivity to MMs with high magnetic charges. Our results are valid for both elementary and composite MMs. The limit from indirect searches for MMs produced by neutron stars [41] is also plotted in Fig. 5. The latter limits become stronger than the results of this work for magnetic charges above $45 g_D$.

In conclusion, the CMS beam pipe was exposed to $174.29 \mu\text{b}^{-1}$ Pb–Pb collisions at 2.76 TeV center-of-mass energy per collision in December 2011. The beam pipe acquired by MoEDAL from CMS was scanned for the presence of trapped magnetic charges using a SQUID magnetometer. No signal candidates were observed. The advantages of the ultraperipheral heavy-ion collisions and close proximity to the interaction point have enabled us to exclude, at 95% C.L., the existence of composite or point-like MMs with masses up to 80 GeV, providing the strongest available constraint for magnetic charges from 2 to $45 g_D$.

Acknowledgments. We thank CERN for the LHC operation, the CMS experiment for the beam pipe, as well as the support staff from our institutions without whom MoEDAL could not be operated. We acknowledge the invaluable assistance of the CMS collaboration. Computing support was provided by the GridPP Collaboration, in particular by the Queen Mary University of London and Liverpool grid sites. This work was supported by the UK Science and Technology Facilities Council, via the grants, ST/L000326/1, ST/L00044X/1, ST/N00101X/1, ST/P000258/1, ST/P000762/1, ST/T000732/1, ST/X000753/1 and ST/T000791/1; by the Generalitat Valenciana via the projects PROMETEO/2021/083, CIPROM/2021/054, CIPROM/2021/073, CIA-POS/2021/88; by Spanish MICIN PID2020-113334GB-I00/AEI/10.13039/501100011033, Project PID2021-122134NB-C21 funded by MCIN/AEI/10.13039/501100011033/ FEDER, UE and MCIN/AEI/10.13039/501100011033, European Regional Development Fund Grant No. PID2019-105439 GB-C21; by MICIU via the mobility grant PRX22/00633; by the Physics Department of King’s College London; by NSERC via a project grant; by the V-P Research of the University of Alberta (UofA); by

the Provost of the UofA; by UEFISCDI (Romania); by the INFN (Italy); by the Estonian Research Council via a Mobilitas Plus grant MOBTT5; by a Royal Society Dorothy Hodgkin Fellowship; and by the NSF grant 2309505 to the University of Alabama MoEDAL group. A. Rajantie was also supported by Institute for Particle Physics Phenomenology Associateship. I. Ostrovskiy thanks the Chinese Academy of Sciences (CAS) President’s International Fellowship Initiative (PIFI) for the support.

Data Availability Statement. The data supporting this study are available upon request.

^a Also at Int. Centre for Theoretical Physics, Trieste, Italy

^b Also at Department of Physics, School of Applied Mathematical and Physical Sciences, National Technical University of Athens, Athens, Greece

^c Currently at Institute of High Energy Physics, Beijing, China; Corresponding author: iostrovskiy@ua.edu

- [1] P. A. M. Dirac, Proc. Roy. Soc. Lond. **133**, 60 (1931).
- [2] G. Hooft, Nucl. Phys. B **79**, 276 (1974).
- [3] A. M. Polyakov, JETP Lett. **20**, 194 (1974).
- [4] Y. Cho and D. Maison, Phys. Lett. B **391**, 360 (1997).
- [5] K. Kimm, J. H. Yoon, and Y. M. Cho, Eur. Phys. J. C **75**, 1 (2015).
- [6] J. Ellis, N. E. Mavromatos, and T. You, Phys. Lett. B **756**, 29 (2016).
- [7] N. E. Mavromatos and S. Sarkar, Phys. Rev. D **95**, 104025 (2017).
- [8] S. Arunasalam and A. Kobakhidze, Eur. Phys. J. C **77**, 444 (2017).
- [9] N. E. Mavromatos and S. Sarkar, Phys. Rev. D **97**, 125010 (2018).
- [10] P. Q. Hung, Nucl. Phys. B **962**, 115278 (2021).
- [11] D. Raut, Q. Shafi, and A. Thapa, Eur. Phys. J. C **82**, 803 (2022).
- [12] G. Lazarides and Q. Shafi, Phys. Lett. B **818**, 136363 (2021).
- [13] D. Tong, JHEP **07**, 104 (2017).
- [14] X.-G. Wen and E. Witten, Nucl. Phys. B **261**, 651 (1985).
- [15] N. E. Mavromatos and V. A. Mitsou, Int. J. Mod. Phys. A **35**, 2030012 (2020).
- [16] A. De Roeck, A. Katre, P. Mermoud, D. Milstead, and T. Sloan, EPJ C **72**, 1985 (2012).
- [17] A. De Roeck, H. P. Hächler, A. M. Hirt, M. D. Joergensen, A. Katre, P. Mermoud, D. Milstead, and T. Sloan, Eur. Phys. J. C **72**, 2212 (2012).
- [18] A. Aktas *et al.* (H1 Collaboration), Eur. Phys. J. C **41**, 133 (2005).
- [19] G. R. Kalbfleisch, W. Luo, K. A. Milton, E. H. Smith, and M. G. Strauss, Phys. Rev. D **69**, 052002 (2004).
- [20] G. R. Kalbfleisch, K. A. Milton, M. G. Strauss, L. Gamberger, E. H. Smith, and W. Luo, Phys. Rev. Lett. **85**, 5292 (2000).
- [21] B. Acharya *et al.* (MoEDAL Collaboration), Phys. Rev. Lett. **123**, 021802 (2019).
- [22] B. Acharya *et al.* (MoEDAL Collaboration), Phys. Rev. Lett. **126**, 071801 (2021).

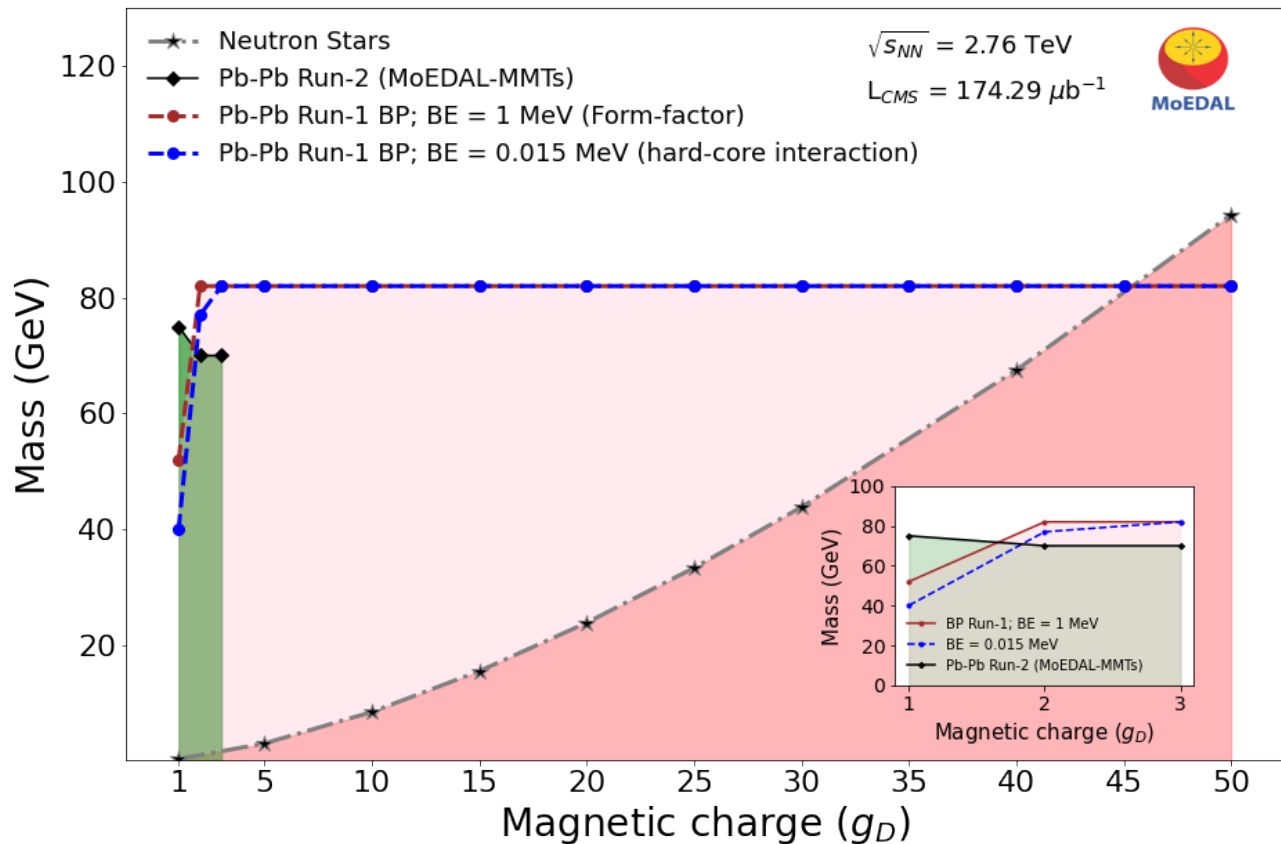


FIG. 5. The 95% C.L. exclusion region for MM production via the Schwinger effect in Pb–Pb collisions at CMS during Run-1 of the LHC. The region shaded in green corresponds to the mass bounds from the MoEDAL search [27]. The insert zooms in on the low-charge region. The limit from indirect searches for MMs produced by neutron stars [28] is also shown, indicating that the current search provides the strongest available limits for charges up to 45 g_D .

- [23] B. Acharya *et al.* (MoEDAL Collaboration), (2023), arXiv:2311.06509 [hep-ex].
- [24] J. Alexandre and N. E. Mavromatos, *Phys. Rev. D* **100**, 096005 (2019).
- [25] E. Witten, *Nucl. Phys. B* **160**, 57 (1979).
- [26] A. K. Drukier and S. Nussinov, *Phys. Rev. Lett.* **49**, 102 (1982).
- [27] B. Acharya *et al.* (MoEDAL Collaboration), *Nature* **602**, 63 (2022).
- [28] O. Gould, D. L. J. Ho, and A. Rajantie, *Phys. Rev. D* **104**, 015033 (2021).
- [29] O. Gould, D. L.-J. Ho, and A. Rajantie, *Phys. Rev. D* **100**, 015041 (2019).
- [30] S. Chatrchyan *et al.* (CMS Collaboration), *J. Instrum.* **5**, T03021 (2010).
- [31] S. Agostinelli *et al.* (Geant4 Collaboration), *Nucl. Instrum. Meth. A* **506**, 250 (2003).
- [32] S. P. Ahlen, *Phys. Rev. D* **17**, 229 (1978).
- [33] S. Cecchini, L. Patrizii, Z. Sahnoun, G. Sirri, and V. Togo, arXiv:1606.01220 (2016), arXiv:1606.01220 [physics.ins-det].
- [34] S. P. Ahlen and K. Kinoshita, *Phys. Rev. D* **26**, 2347 (1982).
- [35] J. Derkaoui, G. Giacomelli, T. Lari, A. Margiotta, M. Ouchrif, L. Patrizii, V. Popa, and V. Togo, *Astropart. Phys.* **9**, 173 (1998).
- [36] K. A. Milton, *Rep. Prog. Phys.* **69**, 1637 (2006).
- [37] L. Bracci and G. Fiorentini, *Nucl. Phys. B* **232**, 236 (1984).
- [38] K. Olausson and R. Sollie, *Nucl. Phys. B* **255**, 465 (1985).
- [39] S. Agostinelli *et al.* (Geant4 Collaboration), *Book For Application Developers* (2017).
- [40] B. Acharya *et al.* (MoEDAL Collaboration), *JHEP* **2016**, 67 (2016).
- [41] O. Gould and A. Rajantie, *Phys. Rev. Lett.* **119**, 241601 (2017).